IS-PORTO 2023 PROCEEDINGS

Proceedings of the 8th International Symposium on DEFORMATION CHARACTERISTICS OF GEOMATERIALS Porto, 3rd - 6th September 2023

Continuous soil deformation measurement and tracking during triaxial testing

Xiaolong Xia[1] and *Xiong* Zhang[2#]

[1]*Geotech Engineering and Testing, Houston, Texas 77396, USA*
[2] *Missouri University of Science and Technology. Department of Civil, Architectural and Environmental Engineering, Rolla, MO 65401, USA*
[#]*Corresponding author: zhangxi@umsystem.edu*

ABSTRACT

Extensive research efforts have been made to measure the soil deformations during triaxial testing. However, continuous soil deformation measurement is still a challenge to researchers since conventional photogrammetry cannot be used for the triaxial test in which the soil specimen is continuously deforming. This paper presents a feasibility study on developing a photogrammetric method to track the evolution of 3-D soil deformations during triaxial testing. Thirteen to sixteen low-cost surveillance cameras are installed to a steel ring around the triaxial test apparatus. The whole triaxial test process is videotaped by these surveillance cameras. The 3-D model of the soil specimen at the initial moment is obtained by processing the first image frame for each video using a structure from motion photogrammetric method. The pixel information and IDs of the points of interest at other moments are tracked through an efficient nearest point search method. A series of triaxial test was performed to validate the concept of the proposed method. Experimental results indicate that the overall reprojection error is less than 1 pixel. The proposed method can potentially be used to track the 3-D localized strain/deformations of the soil specimen at every moment during the triaxial testing.

Keywords: continuous soil deformation measurement; triaxial testing; photogrammetric method; surveillance cameras.

1. Introduction

Measuring the soil deformations during triaxial testing is an important part of characterizing the stress-strain behaviour of soils. A review of the method for volume measurement of soils during triaxial test can be found in Laloui et al. (2006); Zhang et al. (2015); and Lin et al. (2015). It is found out that all existing methods have limitations in measuring the volume-changes of soils (especially for unsaturated soils) during triaxial testing. In recent years, Zhang and co-workers (Zhang et al. 2015; Lin et al. 2015; Fayek et al. 2020; and Xia et al. 2021) developed a photogrammetry-based method which can measure not only the 3-D full-field displacement, but also the absolute volume, tilting and eccentricity of the soil specimen. This method has many advantages over existing methods, such as high accuracy (less than 0.076 mm for point measurement and better than 0.25% for soil volume measurement), low cost (< $ 2K) and both global and localized deformation measurement. While this method is very useful, one limitation is the inability to continuously measure the deformations of the soil in triaxial test in which the soil specimen is continuously deforming. In Zhang et al. (2015), only one camera was used, and the method requires the test to be paused when taking images. However, for many tests, such as the triaxial tests on soils, the soil deformations are continuous. As a result, the tests cannot be paused during the test. Not to mention when using this method to perform dynamic tests. Therefore, there is a clear need to develop a system which can continuously measure the 3-D full-field deformations of soil specimens during triaxial testing.

An alternative method for continuously measuring and tracking the deformations of soil specimen is to use multiple digital SLR cameras. However, generally 12-24 cameras are required, which can cause high cost. On the other hand, the potential of using low-cost security cameras in measuring the volume-changes of unsaturated soils during triaxial testing has been largely unexplored. More recently, a low-cost multi-camera based photogrammetric method (Xia et al. 2022) was proposed to measure the volume-changes of unsaturated soils during triaxial testing. However, continuous soil deformation measurement is still a challenge. The objective of this paper is to overcome the above limitations by using the low-cost security cameras to continuously measure the 3-D full-field deformations of the soil specimens during triaxial testing.

The total cost of the security camera system is about $ 2K (about $ 160 for each camera). One can take full advantage of the automatic data acquisition of the security camera system. However, there are some potential problems raised as summarized as follows: (1) the relatively low-resolution of the security cameras. Most commercially available security cameras have a resolution equal or smaller than 4K. 4K refers to a horizontal display resolution of approximately 4000 pixels. For example, a typical 4K resolution is 3840 pixels by 2160 pixels which is only about half of the digital SLR camera resolution. The low resolution of security cameras can directly cause unfavourable coded target and solid dot recognition and identification results,

which will further influence the subsequent 3-D reconstruction and volume measurement results; (2) the large image distortion. Security cameras are generally designed to keep property safe and need to have a much larger field of view angle to have more coverage of an entire area. These cameras are also referred to as wide angle cameras which often have field of views between 60 and 110 degrees. However, the large field of view often causes large image distortion. Large image distortion without being properly handled can undoubtfully influence the measurement results; (3) the unknown accuracy of the security camera system. Based on the abovementioned discussion, both the low image resolution and large image distortion of security cameras can potentially cause inaccurate coded target and solid dot detection results and 3-D measurement accuracy. Therefore, the accuracy of the security cameras system is one of the major concerns that needs to be addressed; (4) a high-efficiency computer program is required to process the large video files. This study aims at addressing each of the above issues and demonstrating the potential of the proposed method to continuously track the 3-D localized strain/deformations of the soil specimen during the triaxial testing.

2. Proposed Method

2.1 System Setup

The multi-camera system setup is shown in Fig.1. A total of thirteen to sixteen low-cost security cameras are used in this study. It is noted that the cameras in this study are used as representative security cameras to demonstrate the ability of the proposed method and one can have more options to use other security cameras for the proposed method. All the thirteen cameras are controlled and managed by a 16-channel 4K UHD Network Video Recorder (NVR) from Lorex. The NVR with 4TB hard disk drive (HDD) can record from and manage the sixteen security cameras at resolutions up to 3840 × 2160. Equipped with two SATA ports, this NVR can support up to 16TB of internal storage (4TB is preinstalled). H.265 and H.264 video codecs keep file sizes manageable while maintaining the best quality possible. The NVR offers a reliable way to achieve

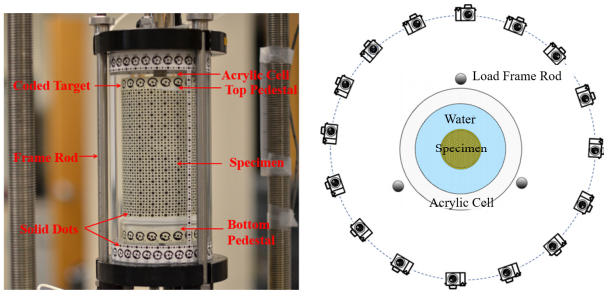

Figure 1. System setup for the proposed method: (a) Setup of the triaxial test system; (b) Top view of camera positions for the multi-camera system (modified from Zhang et a. 2015).

synchronization of image and video generation which is very important in video-based tracking method. Each camera has an 8 MP 1/2.3" image sensor with a focal length of 4.0 mm according to the specifications. It is noted that all these cameras have fixed focal lengths. The lens field of view is 93 degrees. The streaming resolution of the cameras is 3840 × 2160 at 15 fps.

2.2 Coded Target (CT)/Solid Dot Design

Both CTs and solid dots are used in the proposed method. The CT/solid dots design is shown in Fig. 1a. A solid dot is a simple dot that has a much smaller dimension than a CT. When carefully labelled or coded, the solid dot has the same function as the CT. Due to its small dimension, use of solid dots can significantly increase the point density. In Fig. 1a, a total of 92 CTs and 4260 solid dots are posted on the acrylic cell or printed on the rubber membrane. The ID design for these CTs and solid dots are listed in Table 1. In the proposed method, a relatively small number of CTs are used to improve the efficiency and reduce the processing time for target recognition and identification. Automatic recognition and marking of solid dots are generally simpler and faster than CTs as will be explained in later section.

Table 1. Predesigned lookup table for the CTs/solid dots.

Region	Stripe	Start ID	End ID	Number of Points
Pedestal	Top annular CT stripe	1	16	16
	Bottom annular CT stripe	17	32	16
Acrylic cell	Top annular CT stripe	101	130	30
	Bottom annular CT stripe	131	160	30
	Top annular solid dot stripe	161	280	120
	Bottom annular solid dot stripe	281	400	120
	Longitudinal solid dot stripe 1	401	460	60
	Longitudinal solid dot stripe 2	461	520	60
	Longitudinal solid dot stripe 3	521	580	60
Membrane	Annular solid dot stripe	1001	4840	3840
-	-	-	-	Total:4352

2.3 Coded Target (CT)/Solid Dot Detection

Surveillance cameras have larger field of view angles and produce images with larger distortion. Therefore, the surveillance cameras need to be carefully calibrated before any photogrammetric analysis. The procedures for surveillance camera calibration were similar to those for a digital single-lens reflex camera as described in Zhang et al. 2015 and standard camera model was also used. In this study, a Matlab app called the Single Camera Calibrator app was used to calibrate the camera used. The calibration was done by taking 10-20 images of a calibration sheet. The intrinsic (focal length and distortion parameters) and extrinsic (translation vector and rotation matrix) parameters were then calculated by analyzing the camera calibration images.

After the first frame for each video is extracted, the CTs/solid dots detection is performed for each of these images using the target recognition and identification

algorithms. The method in Xia et al. (2021) is adopted to perform CT identification. Fig. 2 shows the automatic recognition and identification of the solid dots on the acrylic cell and membrane.

Simple and fast image processing algorithms for solid dot recognition and decoding have been developed in this study to facilitate the automation and improve the efficiency of the proposed method. After image distortion correction, the image is converted into a binary image. There are a lot of unnecessary and unwanted objects (also referred to as blobs). The solid dots can be correctly recognized by applying the area and roundness criteria. After the solid dots are recognized, another image processing algorithm has been developed to automatically label each solid dot with a unique ID number (also referred to as decoding or identification). The decoding of the solid dots is illustrated in Fig. 2. Then, by comparing the predicted locations and the pixel locations of all the solid dots the accurate locations for each solid dot can be obtained and the IDs can be easily assigned.

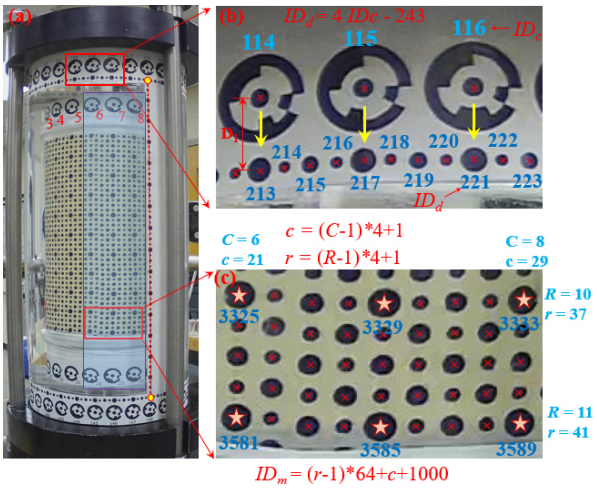

Figure 2. Automatic recognition and identification of the solid dots on the acrylic cell and membrane: (a) a typical triaxial image; (b) an enlargement of the image patch on the acrylic cell; and (c) an enlargement of the image patch on the membrane.

Fig. 2a is a typical triaxial cell image. A small image patch on the top annular CT/solid dot stripe is selected to illustrate the proposed solid dot decoding method. The enlargement of this image patch is shown in Fig. 2b. Assume the CT locations (denoted by the cross at the center of the CT) and IDs (114, 115, and 116) are already obtained using the CT identification algorithm proposed in Xia et. 2021, the solid dots locations can be easily predicted by moving the CT centers down a distance of D1. D1 can be obtained from the predesigned geometrical information regarding the relative location between the CTs and solid dots. Before the CTs and solid dots are posted to the acrylic cell, how relative location of each CT and solid dot compared with other CTs and solid dots are carefully designed and known. One can take advantage of this redesigned geometric information to predict the solid dot centers. Then, a nearest point search is conducted to search the nearest point in the initial solid dot detection results compared with the predicted solid dot location. Therefore, the accurate solid dot locations can be obtained. To label each of the solid dots automatically, the following equation is applied:

$$ID_d = 4\,ID_c - 243 \quad (1)$$

where ID_c represents the ID number of the CT, and ID_d represents the ID number of the solid dot that corresponds to the CT. For example, after translating CT 114 to the solid dot directly below CT 114, an ID number 213 is automatically assigned to this solid dot.

Each of the solid dots that is directly below the CTs are slightly larger than other solid dots as shown in Fig. 2b. These solid dots are labelled by using the simple equation (1). The locations and ID numbers of the smaller solid dots that are between the larger solid dots can be readily obtained by one-dimensional interpolation. It is worth noting that all the solid dots are automatically labelled without using complex target identification algorithms. Instead, simple equation (1) and 1-D linear interpolation are applied, which can significantly reduce the image processing time and reduce the chance of errors.

Similarly, the solid dots on the longitudinal stripe as shown in the vertical line in Fig. 2a can also be recognized and identified based on the CT recognition and identification results. The locations of the uppermost and downmost solid dots on this stripe can be predicted and refined according to the pixel coordinates of the CTs directly above or below the two solid dots. The solid dots in the middle of the longitudinal stripe can be obtained using a linear interpolation technique.

Fig. 2c shows an enlargement of an image patch on the membrane. This image patch is selected to illustrate how the solid dots on the membrane are automatically recognized and identified. Firstly, based on the IDs of CTs on the top and bottom pedestals, the pedestal CT pairs are found. A pedestal CT pair means that the CT IDs difference between the two CTs is 16 and the paired CTs are located at similar horizontal locations but on the top and bottom pedestals, respectively. From each CT pair, a polygon can be defined to include all the solid dots on the membrane. Then, the eleven largest solid dots are detected by selecting eleven solid dots with the largest area. This process is repeated for each of the pedestal CT pairs and all the larger solid dots on the membrane can be obtained. The next step is to detect the smaller solid dots through a 2-D interpolation method based on the larger solid dots. Finally, the ID numbers of the solid dots on the membrane are automatically assigned by using the following equations:

$$c = (C\text{-}1)\times 4 - 1 \quad (2)$$

$$r = (R\text{-}1)\times 4 - 1 \quad (3)$$

$$ID_m = (r\text{-}1) \times 64 + c + 1000 \quad (4)$$

where C is the column number of the pedestal CT pairs which is also the CT IDs on the top pedestal; R is the row number of the large solid dots without considering the small solid dots ranging from 1-11. c and r are the column number and row number of the solid dots on the membrane. ID_m is the ID number of the solid dots on the membrane. In Fig. 2c, the C, R, c, r, and ID_m values of the six large solid dots are presented as an example.

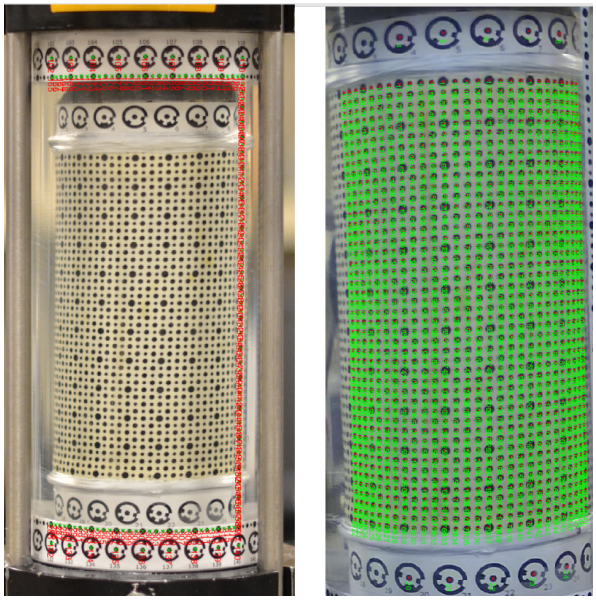

(a) (b)

Figure 3. CTs/solid dots detection results: (a) detection results for the outside of the acrylic cell; and (b) detection results for the inside of the acrylic cell (membrane).

The CT and solid dot IDs and pixel information serve as input to a 3-D reconstruction program to obtain the 3-D model of the acrylic cell in the air. In this study, a structure from motion photogrammetric method is adopted to obtain the 3-D model of the acrylic cell. The soil specimen is immersed in water during triaxial testing, and the refraction effect needs to be addressed. To deal with the refraction problem, a ray tracing technique (Zhang et al. 2015) was adopted to obtain the 3-D model of the triaxial soil specimen in water. A scale and a global 3-D coordinate system were also defined in the analysis. All the above- mentioned procedures were completed by a MatLab program developed by the authors so that the computation process is highly automatic and fast. Typical CT/solid dot detection results for outside and inside of the acrylic chamber are shown in Figs. 3a and 3b, respectively.

2.4 Tracking the Target Locations

All the frames except for the first frames are processed by a tracking method. An efficient target tracking method is necessary due to at least two reasons: (1) the deformation of the soil specimen is very small comparing the two adjacent frames. The selected security cameras have a frame rate of 15 frames per second. Therefore, the difference between the two adjacent frames is very small. There is no need to compute the target locations by using a "brute-force" method, for example, relying on solely the conventional target recognition and identification algorithms to compute the pixel coordinates and 3-D locations of the CTs/solid dots. A simple tracking technique should be sufficient to obtain the target locations in a much easier way. (2) Depending on the total testing period and frame rate, the video files can be very large, and thousands of frames need to be processed. Conventional "brute-force" target recognition and identification algorithms which compute the pixel information and ID numbers for each of the targets can be extremely inefficient.

In this paper, an efficient and fast target tracking method is utilized to determine the target locations. Fig. 4 shows a schematic plot of the target tracking method.

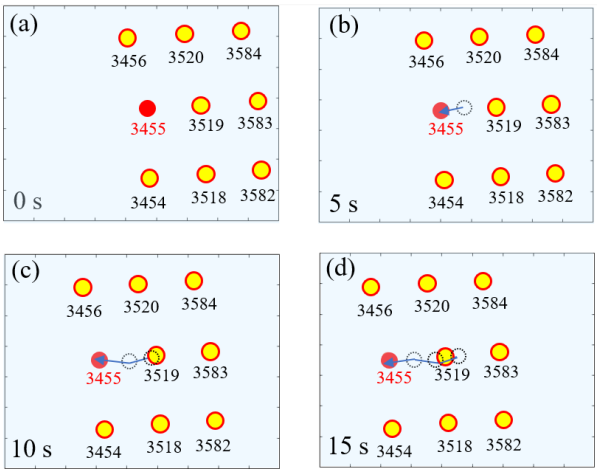

Figure 4. Schematic plot of the target tracking method: (a) target locations at time = 0s; (b) target locations at time = 5s; (c) target locations at time = 10s; and (d) target locations at time = 15s.

The initial pixel locations of the targets for the first frame (time = 0s) are obtained by using the method described previously and are shown in Fig. 4a. The next frame to be processed depends on the time step we select for video processing. In our case, a time step of 5s is selected so that obvious displacements of the targets can be observed in the figure. Fig. 4b represents the pixel locations of the targets at time T = 5s. The shaded circles represent the pixel coordinates of the targets at current moment (T = 5s), while the circle with dotted line denotes the target location for solid dot 3455 at previous moment (T = 0s). To predict the new location of each target, a nearest point search is performed to find the nearest point between the previous location of this target and all the solid dots at the current moment. Thus, the accurate pixel location of the target at the current moment can be obtained. The IDs of these solid dots keep the same during the tracking process. Figs. 4c and 4d show the pixel locations of the targets at moments T = 10s and T = 15 s, respectively. The changes in pixel location for solid dot 3455 are continuously tracked. This simple target tracking method saves a lot of processing time. A Matlab program has been developed for tracking and the tracking of targets on each frame takes only about one second.

3. Preliminary Results and Discussion

3.1 Initial 3-D Reconstruction Results

Fig. 5 shows the initial 3-D results for the acrylic cell and camera stations for the first frames which represent the initial moment T = 0s. The positions of the security cameras and 3-D model of the acrylic cell are obtained using the proposed method. It was found that the mean reprojection error for the 3-D reconstruction is only 0.29 pixel. Mean reprojection error indicates the difference between points' calculated 3-D position and their marked

position on images. The small mean reprojection error obtained indicates that the proposed method is accurate in terms of the 3-D results. Since the security cameras are installed on a ring and are approximately equally spaced, the camera stations presented in Fig. 5 agree well with the actual camera stations. It can also be seen that the top view of the 3-D model of the acrylic cell shows a very good circular shape. This agrees very well with the actual circular shape of the acrylic cell as well. Therefore, the proposed method gives accurate and promising results regarding the 3-D model of the acrylic cell in the air.

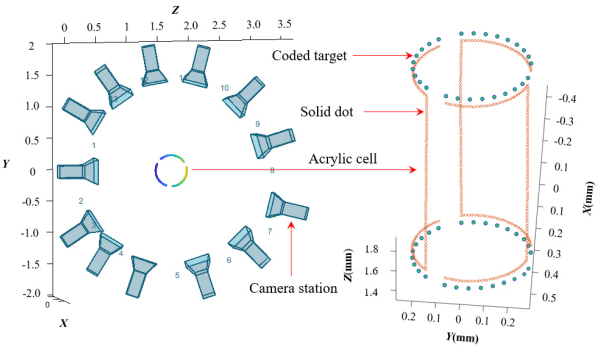

Figure 5. 3-D reconstruction results in the air for the first frames.

3.2 Post-processing and Ray Tracing Results

After refraction correction, the 3-D model of the soil specimen in the water is also obtained. Fig. 6 shows the ray tracing results and the top view of the 3-D model of the soil specimen. A representative solid dot on the membrane is used as an example. For this point (solid dot), five rays are used simultaneously to determine the 3-D coordinates of this point in space. It is also found most of the points on the membrane are determined by five rays. This indicates that thirteen security cameras are sufficient to ensure reliable 3-D results for the soil specimen in water. The 3-D models of the acrylic cell and soil specimen are shown in Fig. 6. The 3-D information of a total of 2624 dots was obtained. Comparing with previous methods (Zhang et al. 2015; Lin et al. 2015; Fayek et al. 2020; and Xia et al. 2021), a much denser point cloud is generated. Therefore, more representative and accurate soil deformation can be obtained by the proposed method.

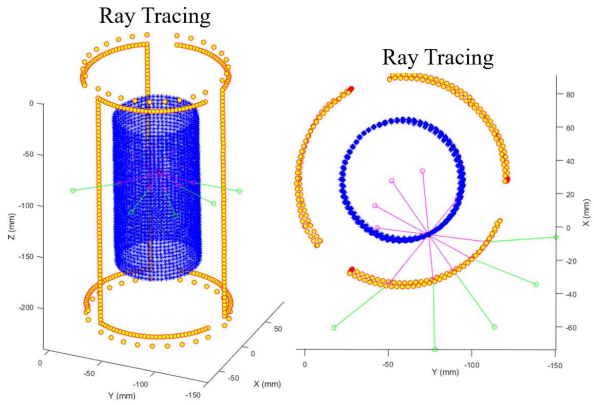

Figure 6. 3-D models of the acrylic cell and soil specimen.

After the 3-D coordinates of the solid dots on the soil specimen are obtained, post-processing can be performed to generate 3-D meshes for the soil specimen. Then, a method for determining the absolute volume of the soil specimen in Fayek et al. (2020) can be adopted to calculate the absolute volume of the soil. By comparing the analysis results between different moments, the volume-changes for the specimen can be obtained.

3.3 Continuous 3-D Deformation Measurement and Tracking

One major advantage of the proposed method is its ability to continuously measure and track the 3-D deformations of the soil specimen during the whole triaxial testing. Fig. 7 shows the 3-D models of the soil specimen different moments and axial displacements. It is worth noting that although only the 3-D models at six moments are presented in Fig. 7, the 3-D results at any time during the triaxial testing are obtained and made into a movie to display the whole 3-D deformation process.

As can be seen in Fig. 7, the deformations became larger and larger over time. It was also found that the deformations of the soil specimen are non-uniform. The deformations at the lower portion of the specimen are much larger than those at the top of the soil specimen.

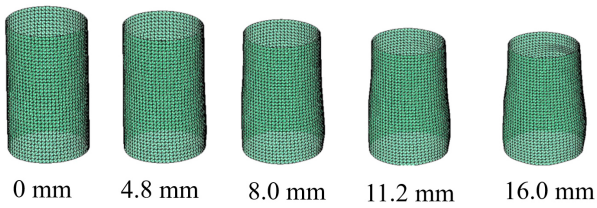

Figure 7. 3-D models of unconfined compression test soil specimen at different axial deformations.

The proposed method can measure both the global and localized deformations of the soil specimen. The results presented in this paper shows the preliminary 3D reconstruction results. Although the standard camera calibration parameters are used in this study, the proposed method still shows promising 3-D reconstruction and ray tracing results. More accurate results regarding the 3-D models of the acrylic cell and soil specimen can be expected in the future work. The preliminary results regarding the 3-D model of acrylic cell and soil specimen can also be used in the postprocessing processes to obtain the absolute volumes and volume changes of the soil specimen during triaxial testing and these results will be reported in the future work.

4. Conclusions

This paper presents a feasibility study on developing a multi-camera-based photogrammetric method which can measure the continuous deformations of both saturated and unsaturated soils during triaxial testing. The following conclusions are made:

(1) The preliminary results indicate that the proposed method can obtain accurate 3-D model of the soil specimen using relatively low-cost security cameras. The large image distortion caused by the wide-angle security cameras is corrected by camera calibration. The mean reprojection error is only 0.29 pixel. Each security

camera costs only about $ 160 and the muti-camera system costs about $ 2K.

(2) The proposed method can be used to track the 3-D localized strain/deformations of the soil specimen at every moment during the triaxial testing. It is found that the deformations of the soil specimen are non-uniform. The lower part of the specimen experienced larger deformations.

(3) The proposed method is highly efficient and automatic. All the computation is conducted by a computer program. The tracking of each target takes only about one second.

References

Fayek, S. Xia, X., Li, L., and X. Zhang, Photogrammetry-Based Method to Determine the Absolute Volume of Soil Specimen during Triaxial Testing. Transportation Research Record, 2674(8), 206-218. (2020)

Laloui, L., Peron, H., Geiser, F., Rifa'i, A., and Vulliet, L. Advances in volume measurement in unsaturated triaxial tests. Soils Found 46(3):341–349. (2006)

Lin, L., Zhang, X., Chen G., and Lytton, R. Measuring unsaturated soil deformations during triaxial testing using a photogrammetry-based method." Canadian Geotechnical Journal, 53(3), 472-489. (2015)

Nishimura, S. Characterisation of soil deformation over wide strain ranges in triaxial test with high-precision stereophotogrammetry. Géotechnique: 1-16. (2022)

Xia, X., Fayek, S., and Zhang, X. Use of Low-Cost Security Cameras to Measure the Volume Changes of Unsaturated Soils during Triaxial Testing. Geo-Congress 2022. (2022)

Xia, X. Zhang, X., Fayek, S., and Zhao, Z., A Table Method for Coded Target Decoding with Application to 3-D Reconstruction of Soil Specimens during Triaxial Testing. Acta Geotechnica. 16 (2021): 3779-3791. (2021)

Zhang X, Li L, Chen G, et al. A photogrammetry-based method to measure total and local volume changes of unsaturated soils during triaxial testing. Acta Geotechnica, 2015, 10: 55-82.